aerospace

MDPI

Article

Improved Wall Temperature Prediction for the LUMEN Rocket Combustion Chamber with Neural Networks

Kai Dresia [1,*], Eldin Kurudzija [1], Jan Deeken [1,2] and Günther Waxenegger-Wilfing [1,3]

[1] Institute of Space Propulsion, German Aerospace Center (DLR), 74239 Lampoldshausen, Germany; eldin.kurudzija@dlr.de (E.K.)
[2] Institute of Jet Propulsion and Turbomachinery, RWTH Aachen University, 52062 Aachen, Germany
[3] Institute of Computer Science, University of Würzburg, 97070 Würzburg, Germany
* Correspondence: kai.dresia@dlr.de

Abstract: Accurate calculations of the heat transfer and the resulting maximum wall temperature are essential for the optimal design of reliable and efficient regenerative cooling systems. However, predicting the heat transfer of supercritical methane flowing in cooling channels of a regeneratively cooled rocket combustor presents a significant challenge. High-fidelity CFD calculations provide sufficient accuracy but are computationally too expensive to be used within elaborate design optimization routines. In a previous work it has been shown that a surrogate model based on neural networks is able to predict the maximum wall temperature along straight cooling channels with convincing precision when trained with data from CFD simulations for simple cooling channel segments. In this paper, the methodology is extended to cooling channels with curvature. The predictions of the extended model are tested against CFD simulations with different boundary conditions for the representative LUMEN combustor contour with varying geometries and heat flux densities. The high accuracy of the extended model's predictions, suggests that it will be a valuable tool for designing and analyzing regenerative cooling systems with greater efficiency and effectiveness.

Keywords: neural network; surrogate model; heat transfer; machine learning; LUMEN; rocket engine; regenerative cooling

Citation: Dresia, K.; Kurudzija, E.; Deeken, J.; Waxenegger-Wilfing, G. Improved Wall Temperature Prediction for the LUMEN Rocket Combustion Chamber with Neural Network. *Aerospace* **2023**, *10*, 450. https://doi.org/10.3390/aerospace10050450

Academic Editor: Qingfei Fu

Received: 4 April 2023
Revised: 8 May 2023
Accepted: 11 May 2023
Published: 12 May 2023

1. Introduction

Regenerative cooling is a critical technology for ensuring the safe and efficient operation of rocket engines. In this system, fuel or oxidizer is pumped through cooling passages in the combustion chamber wall to reduce the wall temperature and protect it from thermal damage. The accurate prediction of heat transfer between the combustion chamber wall and cooling channel is essential for the design of an effective regenerative cooling system. In this paper, we focus on the challenges of predicting heat transfer in regeneratively cooled combustion chambers using liquid methane as the coolant.

Liquid methane has many advantages as a rocket engine fuel, but it also presents significant challenges for heat transfer prediction. Modeling the heat transfer on the cooling channel side and estimating the maximum structure temperature is more difficult than for hydrogen as coolant [1]. Methane is usually at supercritical pressure inside the cooling channels and heats up from subcritical to supercritical temperature. As a result, the Widom line is crossed near the critical point where small variations of the temperature or the pressure have a great impact on the thermodynamic properties of methane. In addition the roughness of the cooling channel walls and changes in the channel geometry also influences the heat transfer processes.

In this paper, we present an extension of our data-based surrogate model for heat transfer prediction in regenerative cooling systems [2–8]. The model was originally developed for straight cooling channels and accurately predicts the maximum wall temperature based on mass flow, heat flux density, channel geometry, thermodynamic state of the fluid,

and channel wall roughness with a mean prediction error of only 16 K for various different temperature and pressure ranges. The model was trained by using results of computational fluid dynamics (CFD) simulations for channel segments with constant geometry. The calculation time could be reduced by a factor of 1000 compared to CFD.

In this study, we extend the existing model to account for curved cooling channels and test it on the representative combustion chamber contour of the LUMEN engine [9]. To achieve this, we use a simple and somewhat naive approach of training the model using data from simulations for cooling channel segments with a constant radius of curvature. This means that the training data does not include changes in channel area, aspect ratio, or curvature, which exist in realistic combustion chamber cooling channels. Despite this limitation, we observe a noticeable improvement in the performance of the model.

However, it is not surprising that a certain prediction error remains. To further enhance the quality of the model, we propose an approach outlined at the end of the paper that also includes inertia effects. In addition, we are currently conducting ongoing research to systematically integrate experimental data for fine-tuning. In summary, contributions include

- an extension of the model to include curvature effects and fin thickness variation
- a detailed investigation of the reaming deviations
- an evaluation of the predictive accuracy for the LUMEN combustion chamber
- a proposed approach for integrating inertia effects into the surrogate model.

2. Heat Transfer Modeling

The prediction of heat transfer for methane flowing in cooling channels of a regeneratively cooled combustion chamber has proven challenging in the past as undesired phenomena, e.g., pseudo-boiling or heat transfer deterioration, influence the heat transfer [10]. The occurrence of these phenomena is affected by many different factors such as the aspect ratio of the cooling channel [11], the ratio of heat flux and mass flow rate or the roughness of the cooling channel surface [1]. The following sections briefly describe the flow in straight and curved cooling channels and the general idea of Nusselt-number correlations. This overview is taken from a previous work by Dresia [3].

2.1. Flow in Curved Cooling Channels

In real rocket applications heat transfer takes place in straight cooling channels in the cylindrical segment and in curved passages at the nozzle throat. Due to the converging-diverging shape of the thrust chamber assembly, both concave and convex asymmetric heated channels are present. In contrast to straight channel flows, a radial pressure gradient exists in curved channels caused by centrifugal forces, which induce recirculation phenomena in the flow. These secondary flows enhance the convective heat transfer at the channel surface [12].

This enhancement is a result of vortices which increase the flow mixing. Due to centrifugal and inertia forces, the fluid in the channel center moves towards the outer wall, whereas fluid close to the side walls is inhibited from mixing through viscous effects at the wall. Thus, it is forced to the inner wall. The resulting vortices are called Dean vortices. The Dean number

$$De = Re\sqrt{\frac{D_\mathrm{h}}{2R_\mathrm{c}}} \tag{1}$$

is a dimensionless quantity which describes the ratio between the product of inertial and centrifugal forces to viscous forces. A large Dean number, as a result of high Reynolds numbers Re, a large hydraulic diameter of the channel D_h or small radii of curvature R_c, indicates strong vortices, which enhance the fluid mixing. The radius of curvature equals the radius of the circular arc which best approximates the curve at that point. For concave heated channels ($R > 0$), the secondary flow transports cold fluid to the heated wall and therefore reduces wall temperatures. For convex heated channels ($R < 0$), hot fluid from

the wall is transported away by those vortices. According to [13], the expected radius of curvature for operational engines is in the range of

$$R \approx (0.5 \ldots 1.5) \cdot r_t, \tag{2}$$

where r_t is the radius of the nozzle throat.

In a numerical study, Pizzarelli et al. [11] investigated the influence of concave and convex heated channels with high aspect ratios and different curvatures for supercritical hydrogen. Their results indicate that heat transfer is enhanced for both concave and convex heated channels, however the pressure drop is higher compared to straight channels.

2.2. Nusselt Number Correlations

A widely used approach to estimate the heat transfer coefficient for cooling channel flows is based on the Nusselt correlation. The Nusselt number Nu is defined as the ratio of convective to conductive heat transfer at a boundary in a fluid:

$$Nu = \frac{\alpha_{cc} D_h}{\lambda_b}, \tag{3}$$

where α_{cc} is the cooling side heat transfer coefficient, D_h the hydraulic diameter of the cooling channel, and λ_b the bulk thermal conductivity of the coolant. For flow regions far away from the inlet and $0.7 < Pr < 120$, $10{,}000 < Re < 120{,}000$, the Nusselt number can be estimated with the Dittus-Boelter correlation [14]:

$$Nu = 0.0023\, Re^{0.8} Pr^{0.4} \tag{4}$$

Due to their low numerical costs, semi-empirical correlations are widely used for heat transfer modeling in liquid propellant rocket engines. However, most correlations depend on the thermodynamic and transport properties of the fluid, so they are only valid for small heat fluxes and thermodynamic regimes. Research is ongoing to improve the accuracy and validity range of these equations, especially for methane [15], e.g., by adding a velocity profile correction term [16].

Future cost saving measures and the importance of a high cooling channel efficiency will pose significant new challenges for simple semi-empirical correlations: Additive manufacturing technology enables more complex cooling channel geometries and heat enhancing techniques, e.g., flow wedges within the cooling channel, make the prediction of heat transfer even more difficult. To make matters worse additive manufacturing leads to a higher surface roughness and the increased friction fundamentally changes the heat transfer processes. As a consequence, the commonly used assumption for heat transfer prediction at low roughness may lead to larger errors if extended to high roughness channels [17].

In addition, there are further effects that complicate the heat transfer modeling. Examples include the influence of variable cross-sections [18] and even the acceleration of the launch vehicle [19]. This means that complex, three-dimensional CFD simulations are regaining importance over empirical correlations. The higher numerical costs of CFD poses a major challenge for design optimization and multidisciplinary system studies with multiple operation regimes. For a critical review of the main trends inferred by numerical simulations the reader is referred to the work by Nasuti and Pizzarelli [1].

2.3. Data-Based Surrogate Model for Wall Temperature Prediction

The main disadvantage of high-fidelity CFD calculations is that they are not suitable for design space exploration and extensive sensitivity analysis due to their large calculation effort. Surrogate models, for example neural networks [20], can alleviate this burden. Based on training data, characteristic model parameters called weights and biases of the neural networks can be optimized to learn a desired mapping. Architectures with multiple hidden layers enable the creation of accurate surrogate models even for high-dimensional problems.

In recent years, data-based modeling techniques are studied for various applications in the aerospace segment, for example for the design of rocket injector elements [21] or cooling channels [2,22], and for different flow phenomena [23,24].

An accurate neural network based surrogate model for the maximum wall temperature along a straight cooling channel was developed by Waxenegger-Wilfing et al. [2]. For training data from approximately 20,000 CFD simulations of simple straight channel segments with constant geometry and heat flux density were used. The neural network has a fully connected, feed-forward architecture with 4 hidden layers and 408 neurons per layer, which is schematically shown in Figure 1. The main limitation of the developed model is that it lacked the influence of curvature and assumed a constant cooling channel fin thickness of 1 mm.

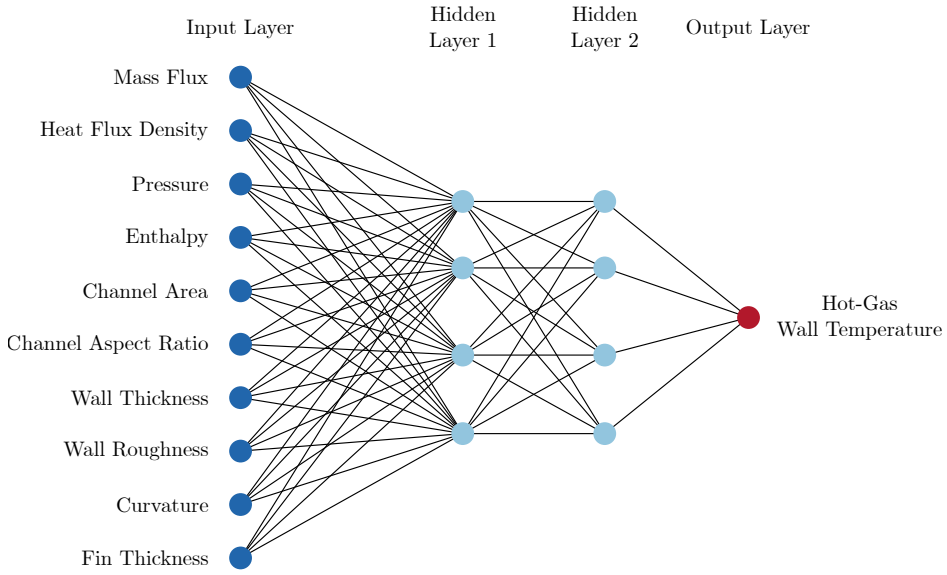

Figure 1. Schematic network architecture; extended with curvature and fin thickness as input.

2.4. Complete Surrogate Model for Cooling Channel Flow

Further equations are required to supplement the neural network and calculate the stream-wise development of thermodynamic properties. A physical model for the development of coolant pressure and enthalpy was implemented in a previous work [2] and validated against CFD. The model is now shortly summarized: The Darcy-Weisbach equation can be used to to estimate the pressure loss in a channel segment of length Δz:

$$\Delta p = \frac{1}{2} f \rho_\mathrm{b} v_\mathrm{b}^2 \frac{\Delta z}{D_\mathrm{h}}, \tag{5}$$

Here f is the so called friction factor, ρ_b is the bulk density of the coolant, v_b is the bulk flow velocity and D_h is the hydraulic diameter of the channel. The friction factor f can be calculated by means of a simple empirical correlation valid for all Reynolds numbers [25].

From conservation of energy one can calculate the change of the specific total enthalpy of the fluid over a channel section of length Δz:

$$h_\mathrm{b,tot}(z + \Delta z) = h_\mathrm{b,tot}(z) + \frac{\dot{Q}(z, \Delta z)}{\dot{m}} \quad \text{with} \quad h_\mathrm{b,tot}(z) = h_\mathrm{b,stat}(z) + \frac{1}{2} v_\mathrm{b}(z)^2, \tag{6}$$

where z is the stream-wise coordinate, $h_\mathrm{b,stat}$ the specific bulk enthalpy of the fluid, v_b the bulk flow velocity, $\dot{m}$ the mass flow rate and $\dot{Q}$ the overall heat flow rate in the channel segment. Incorporating a mass continuity equation and a suitable equation of state, or utilizing the NIST database, yields a comprehensive surrogate model.

3. Surrogate Model Including Curvature and Fin Thickness Effects

The orginal neural network for wall temperature prediction is extended to curvature effects and the variation of the fin thickness. This is achieved by including the reciprocal radius of curvature and the fin thickness as an input variable Figure 1. These enhancements are necessary for applying the model to realistic cooling channel designs with changing curvature and fin thickness. Compared to the previous work, the flow length is no longer an input because it did not improve the predictive quality of the test cases examined.

3.1. Data Generation

The data set from the previous work is extended with additional CFD calculations for curved cooling channels and channels with different fin thicknesses. For this purpose, both concave and convex cooling channels with different geometries, heat flows and thermodynamic states of the cooling medium are calculated. Each CFD simulation is performed for a channel segment with constant curvature and fin thickness.

Figure 2 illustrates the computational model of the curved cooling channel. Straight inlet and outlet sections with a length of 80 mm ensure that the flow in the curved section is not affected by numerical boundary conditions. The relative curvature, which is the radius of curvature divided by the hydraulic diameter of the channel, ranges from 16 to 54.

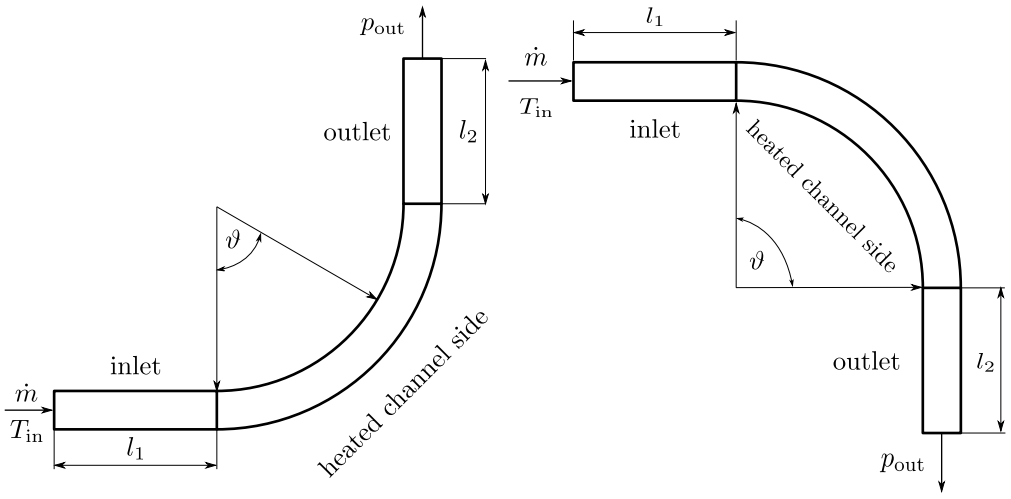

(**a**) Concave heated channel (**b**) Convex heated channel

Figure 2. Curved cooling channel geometry with straight inlet and outlet [3].

We use Ansys CFX 18.0 and mesh the models with Ansys ICEM similarly as in the previous work Waxenegger-Wilfing et al. [2], which is based on the work by Haemisch [26]: The channel flow is modeled as a compressible, stationary problem, while buoyancy and gravitational forces are neglected. Turbulence is computed according to the two-equation shear stress transport (SST) model. In stream-wise direction, no heat flux ($\dot{q} = 0\,\mathrm{W\,m^{-2}}$) is applied for the first 80 mm of the channel to obtain a fully developed flow and velocity boundary layer. The channel surface is modeled as a rough wall with different values for the surface roughness and a no-slip condition. A mass flow boundary condition and the coolant total temperature are imposed at the fluid inlet. Furthermore, the static pressure is fixed at the domain outlet and a symmetric flow boundary condition assures no mass or energy fluxes across the symmetry plane. For the solid domain, all faces, except the hot gas wall, are modeled as adiabatic walls. Thermodynamic properties of supercritical methane are evaluated with data from the NIST database [27]. The solid domain uses two different material models. Combustion chamber and solid fins consist of a CuCrZr-alloy, which in this case is 99.25% copper, 0.62% chrome and 0.1% zirconium. The galvanic layer is made of copper. Fluid–structure interaction is not considered. To reduce the influence of axial

heat transfer, the thermal conductivity in the stream-wise direction is set to zero for both materials. The mesh independence analysis was conducted in a previous work [26].

The CFD results are processed in the same way as in the previous work. The fluid bulk properties are calculated as mass-flow averaged quantities every 2 mm in stream-wise direction and extended by the associated geometric information, such as cross section area, aspect ratio, wall thickness, wall roughness, radius of curvature and fin thickness as well as mass flux and heat flux density. The maximum wall temperature at the hot gas side, which represents the output, is added.

Due to the need for manual input during the geometry generation and meshing process, we conducted simulations on a total of 9 different curved channel segment geometries and 5 different fin thicknesses for straight segments (as outlined in Tables A1 and A2). It is noteworthy that the neural network was able to learn and generalize effectively from this limited set of geometry variations. The final data set used for training and validation is summarized in Tables 1 and A3.

Table 1. Overview of the training and validation data set.

Channel	|R| [mm]	Fin [mm]	Points [10^6]	MAE [K]
straight	-	1	2.36	5.3
curved	25 to 150	1	0.94	4.4
straight	-	0.75 to 3.5	0.36	5.3
curved	30 to 60	0.75 to 1.5	0.14	5.8

3.2. Training

We use a fully connected, feed-forward network with the same hidden layers (4) and neurons (408) as in our previous work. 95% of the data points are selected for training while the rest is held back for validation. The cost function is given by a mean squared error term plus an extra term for L2 regularization of $\alpha = 0.025$. As a result of the data generation with its manually selected boundary conditions, there are regions with higher and lower data density. Thus, we also use sample weights calculated by kernel density estimation to compensate for the non-uniform distribution of data points.

Table 1 contains the mean absolute error (MAE) for the validation sets, while there are 2.7 million data points for straight cooling channel segments, there are about 1.1 million for curved segments. The data points for a fin thickness unequal to one are also clearly underrepresented.

4. Results

In order to evaluate the performance of the extended surrogate model, we verify whether the model has successfully captured the impact of varying radii of curvature on heat transfer. Additionally, we apply the network to changing cooling channel geometries and heat flux densities that differ from the original data set to quantify any errors resulting from our simplistic data generation process. Finally, we investigate the applicability of the surrogate model to the LUMEN combustion chamber.

4.1. Training and Validation Data

First, we study the training and validation data. The accuracy for both data sets is comparable, i.e., we cannot detect any overfitting of the neural network. Thus, it is sufficient to focus on the averaged accuracy. Table 2 shows the mean absolute error (MAE) as well as the 99th percentile error of different portions of the combined data set. The error for large curvatures is on average 5.6 K, for medium curvatures on average 3.9 K. From this it can be concluded that the wall temperature can be predicted well even for the curved segments. However, the greater the curvature (smaller radius of curvature), the higher the error becomes. The prediction for concave and convex geometries is comparably good.

Table 2. Error on train and validation data for different curvatures.

Curvature	|R| [mm]	MAE [K]	99% [K]
medium	60 to 150	3.9	24
strong	25 to 50	5.6	40
concave	negative	4.4	28
convex	positive	4.4	33

Figure 3 shows the prediction error as function of the flow angle θ of the circular channel segment. A central angle of 0° means the flow enters the curved part of the cooling channel segment. Noticeably the error is significantly larger at the transition from the straight to the curved segment. With larger central angle, the error becomes on average smaller, both for strong and medium curvatures.

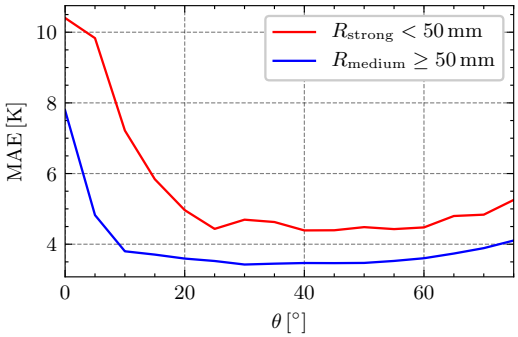

Figure 3. Mean absolute error (MAE) for different radii of curvature over central angle.

It is important to note that the central angle is not equivalent to the flow length. After all, the flow length depends not only on the central angle but also on the radius of curvature.

Now we examine wall temperature predictions for three randomly selected simulations from the train and validation data set. Figure 4 displays the results outcome for a concave segment with a 150 mm radius of curvature, another concave segment with a 25 mm radius of curvature, and a convex segment with a −25 mm radius of curvature. The predictions are highly accurate, with larger errors for large curvatures, i.e., small radius of curvature. Notably, the convex segment exhibits a larger error for a small central angle. In general, the errors are comparable to those observed for straight channels, indicating that the neural network has learned the effects of curvature, despite the underrepresentation of curved data in the training data set.

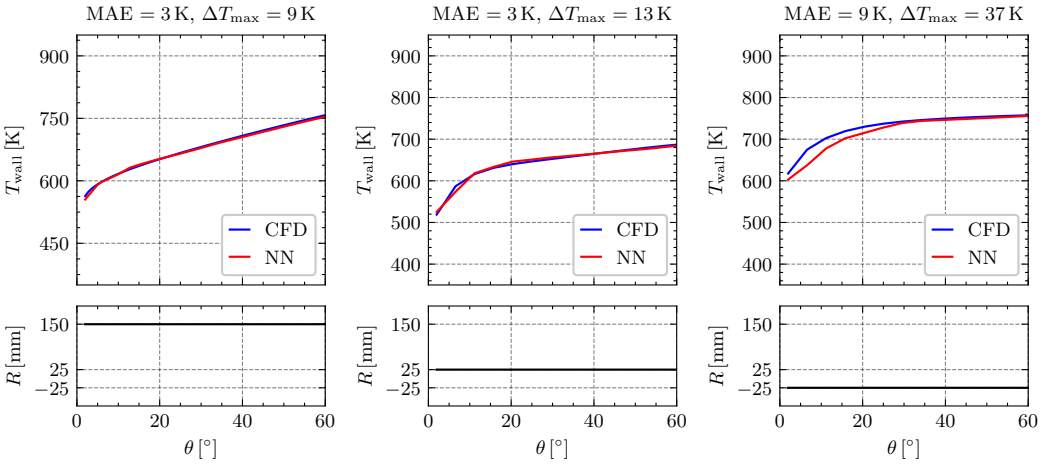

Figure 4. Wall temperature prediction for different radii of curvature.

4.2. Input Variable Changes

This section focuses on an analysis of the extended neural network's performance on segments that significantly differ from those used in training. Specifically, we investigate the impact of varying channel geometries, as well as changes in the heat flux density. This is of particular interest because the training data did not encompass these variations, which have the potential to produce larger prediction errors.

Figure 5a shows the prediction for a heat flux density jump from 35 MW m^{-2} to 70 MW m^{-2} across a distance of 20 mm. Compared to the prediction for constant heat flux densities, the prediction errors are larger with a maximum error of 60 K, which occurs close after the heat flux jump. Similar behavior can be seen in Figure 5b,c for a linear change of the cooling channel height over 20 mm. Interestingly, in the last example, a pronounced error also remains further downstream. In the following sections we will see that the prediction error also increases significantly with changing curvatures for the LUMEN combustion chamber.

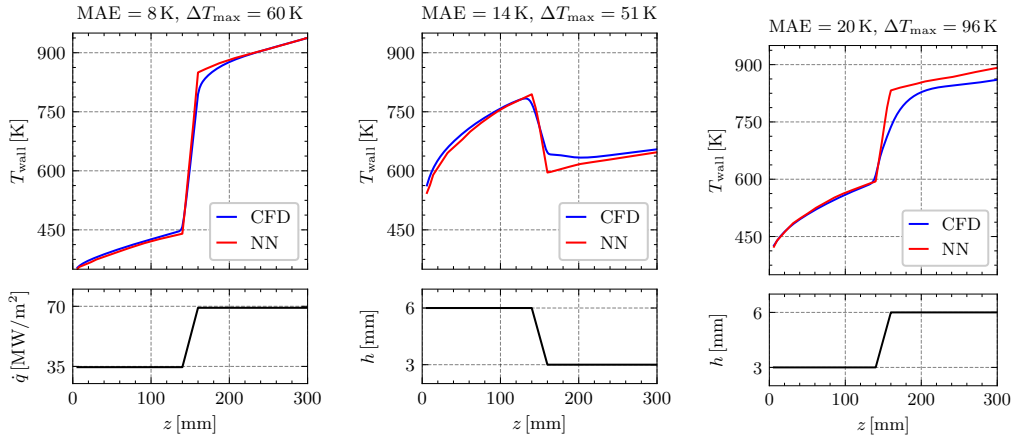

Figure 5. Wall temperature prediction for various straight cooling channels. (**a**) Jump in heat flux density and constant channel geometry. (**b**) Constant heat flux density and jump in channel height. (**c**) Constant heat flux density and jump in channel height.

4.3. LUMEN Cooling Channel Geometry

Now we turn our attention to the representative cooling channel geometries of the LUMEN engine. The significant difference to the previous section is that now the curvature also changes in flow direction. With LUMEN (liquid upper stage demonstrator engine) [9] DLR aims at developing and operating a modular bread-board engine in the 25 kN thrust class for operation at the new P8.3 test facility in Lampoldshausen. The LUMEN engine uses methane as fuel and therefore also as coolant. The flow direction is counter-flow for the nozzle and combustion chamber and co-flow for the nozzle extension (not studied).

The cooling channel height has been optimized at 5 characteristic positions along the combustion chamber length. In between the values are interpolated linearly (see Figure 6). All cooling channels have a constant width of 1 mm with a hot-gas wall thickness of 1 mm. The channel roughness is assumed to be 5 µm.

For this study, the nominal operating point is characterized by a total coolant mass flow of $\dot{m} = 2.6\,\mathrm{kg\,s^{-1}}$ across all 86 channels, an outlet pressure of $p_{\mathrm{out}} = 80\,\mathrm{bar}$, an inlet temperature of $T_{\mathrm{in}} = 120\,\mathrm{K}$, and a heat flux profile $\dot{q}_1$ with a maximum value of $\dot{q}_{\mathrm{max}} = 51\,\mathrm{MW\,m^{-2}}$.

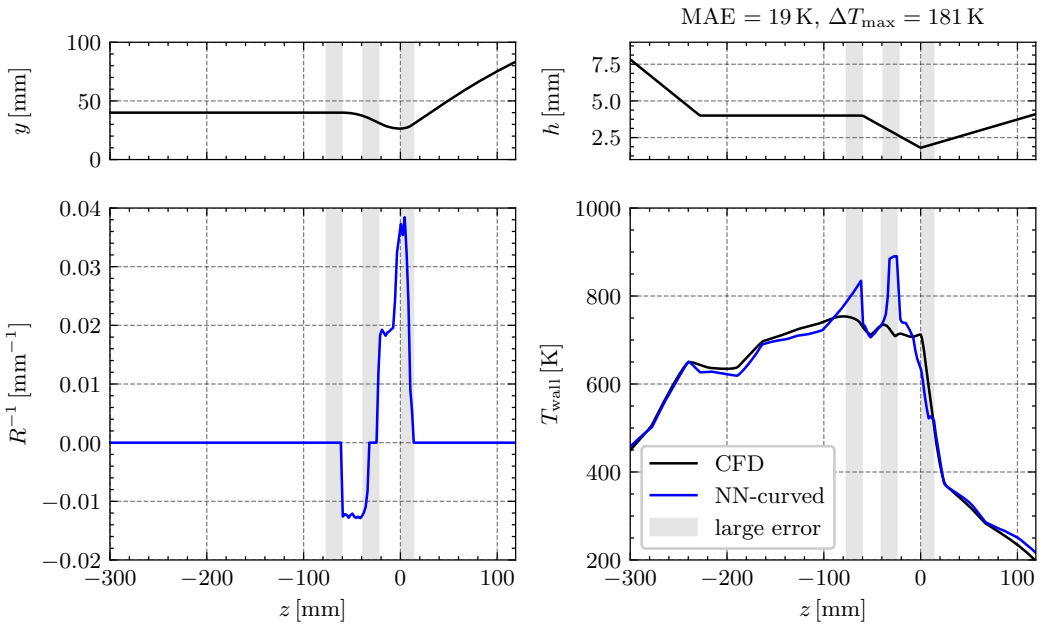

Figure 6. Wall temperature prediction for the LUMEN cooling channel.

4.3.1. Wall Temperature Prediction with Extended Surrogate Model

Figure 6 depicts the prediction of the extended surrogate model from Section 2.4 which includes curvature and fin thickness effects (NN-curved). The prediction is generally accurate with a global MAE of only 19 K, except in the throat region and subsonic part of the nozzle where larger deviations occur. A closer look reveals that the greatest deviations occur in three areas when the radius of curvature changes.

The main source of deviations is observed at abrupt curvature changes where the fluid cannot immediately adapt to the new geometry. This might be due to changes in the thermal and velocity boundary layers, the formation of Dean vortices, and inertia effects within the fluid that cause the previous flow structure to remain for a certain period of time. Since the neural network is not trained to handle changing geometries or abrupt changes in the flow field, it cannot accurately predict the resulting wall temperatures in these regions.

At $z = 15$ mm in the supersonic nozzle, the network produces a larger error as it underestimates the wall temperature. This location marks the transition of the supersonic nozzle's almost straight channels into highly curved channels in the nozzle throat. The network's underestimation of the temperature is due to the high local curvature, which would cause an enhanced heat transfer effect. However, since the curvature changes only slightly before the nozzle throat, the full curvature effects are not fully developed yet.

At $z = -23$ mm in the subsonic part of the nozzle, the curvature changes from convex to concave. Here, the local curvature is temporally zero, but the flow differs from the fully-developed flow in a straight cooling channel due to inertia effects and still remaining vortices from the curved segment before. Hence, the neural network overestimated the wall temperature. The interface between the cylindrical chamber and the subsonic nozzle also exhibits the same behavior.

4.3.2. Curvature Input Modifications

To examine the impact of geometry changes, a preprocessing routine is applied to modify the curvature input data. The curvature is adjusted to remain constant for 15 mm at three specific locations, as shown in Figure 7 and discussed above. Additionally, a moving average is applied to the wall temperature over 5 mm to account for axial heat transfer in the copper. Overall, the preprocessing leads to a significant improvement in the accuracy of the neural network. This indicates, that the larger deviations seen before are indeed cause by inertia effects due to an abruptly changing channel curvature.

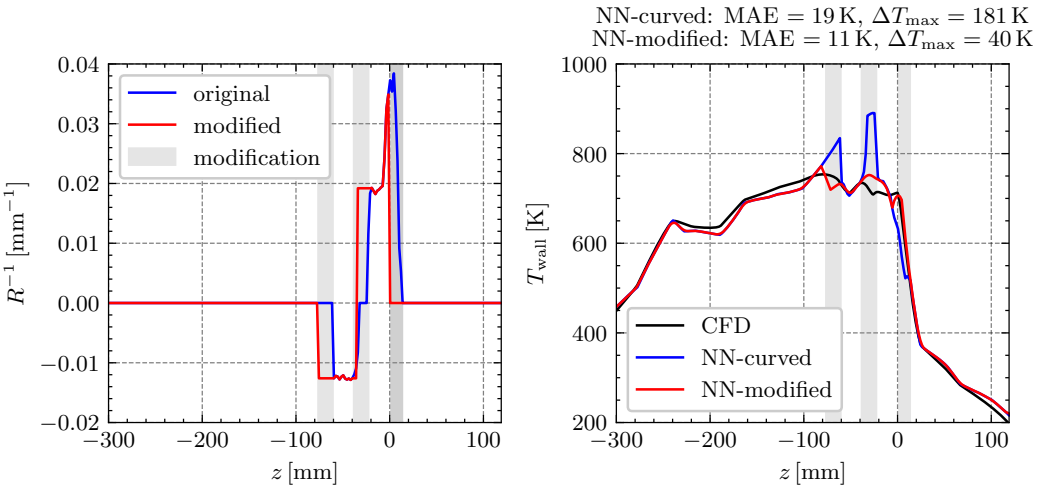

Figure 7. Curvature input modifications to account for inertia effects.

It should be noted, that the appropriate modifications to the curvature depend on various flow characteristics, such as the coolant Reynolds number or density. Therefore, the assumption of modifying the curvature for 15 mm is only valid for operating points near the nominal one. In the outlook section, an approach is described to incorporate these varying inertia effects directly into the neural network architecture.

4.3.3. Influence of Boundary Conditions

Finally, we will study the impact of various flow conditions on the prediction accuracy, by varying the coolant mass flows, the heat flux profile, the channel outlet pressure, and the inlet temperature. First, Figure 8a shows the results for four distinct cooling mass flows. The highest prediction accuracy is achieved for 2.6 kg s^{-1}. The error increases for lower and higher mass flows, as the modifications from Section 4.3.2 are tuned for 2.6 kg s^{-1}. When the mass flow is reduced to 1.7 kg s^{-1}, the extreme temperatures close to the throat lead to a larger error. Additionally, the error increases in the supersonic part of the nozzle for 1.7 kg s^{-1}. We suspect that the larger error may be attributed to the available training data, with the input data being at the boundary of the training data distribution.

Second, Figure 8b illustrates the wall temperature for different heat flux profiles. The neural network is able to predict the general increase in temperature for higher heat fluxes, but it overestimates the temperature in the area at around $z = 50$ mm. This can be attributed to the higher mass flow of 4.3 kg s^{-1}.

Third, in Figure 9a,b the influence of various outlet pressures and inlet temperatures are studied. For inlet temperatures below approximately 200 K, the fluid passes the Widom line in the cooling channel ($p_{crit} = 46$ bar, $T_{crit} = 190.5$ K). At this point, it transitions from a liquid-like to a gas-like state. Passing the Widom line close to the critical point has a large influence on transport properties, such as thermodynamic conductivity or viscosity. For the an inlet temperature of $T_{in} = 250$ K, methan is entirely gas-like and does not cross the Widom-line.

In general, it appears that the neural network has learned how changes in fluid transport properties near the critical point affect the heat transfer. As previously noted, the most significant errors occur in regions of considerable curvature changes, such as the transition from the cylindrical section to the subsonic nozzle. The prediction error in this region is increased due to the close proximity to the critical point at an outlet pressure of 50 bar. Nevertheless, the error is still considered acceptable for most applications.

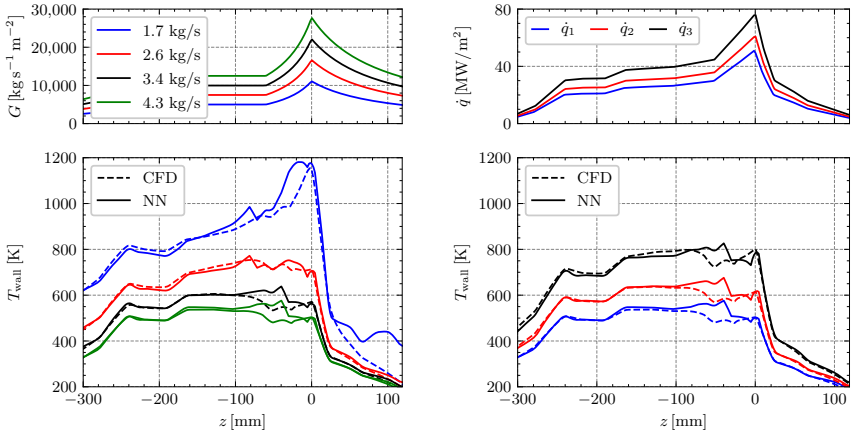

(**a**) (**b**)

Figure 8. Influence of mass flow and heat flux density on the wall temperature prediction. (**a**) Mass flow variations for $p_{\mathrm{out}} = 80\,\mathrm{bar}, \dot{q}_{\mathrm{max}} = 51\,\mathrm{MW\,m^{-2}}, T_{\mathrm{in}} = 120\,\mathrm{K}$. (**b**) Heat flux variations for $p_{\mathrm{out}} = 80\,\mathrm{bar}, \dot{m} = 4.3\,\mathrm{kg\,s^{-1}}, T_{\mathrm{in}} = 120\,\mathrm{K}$.

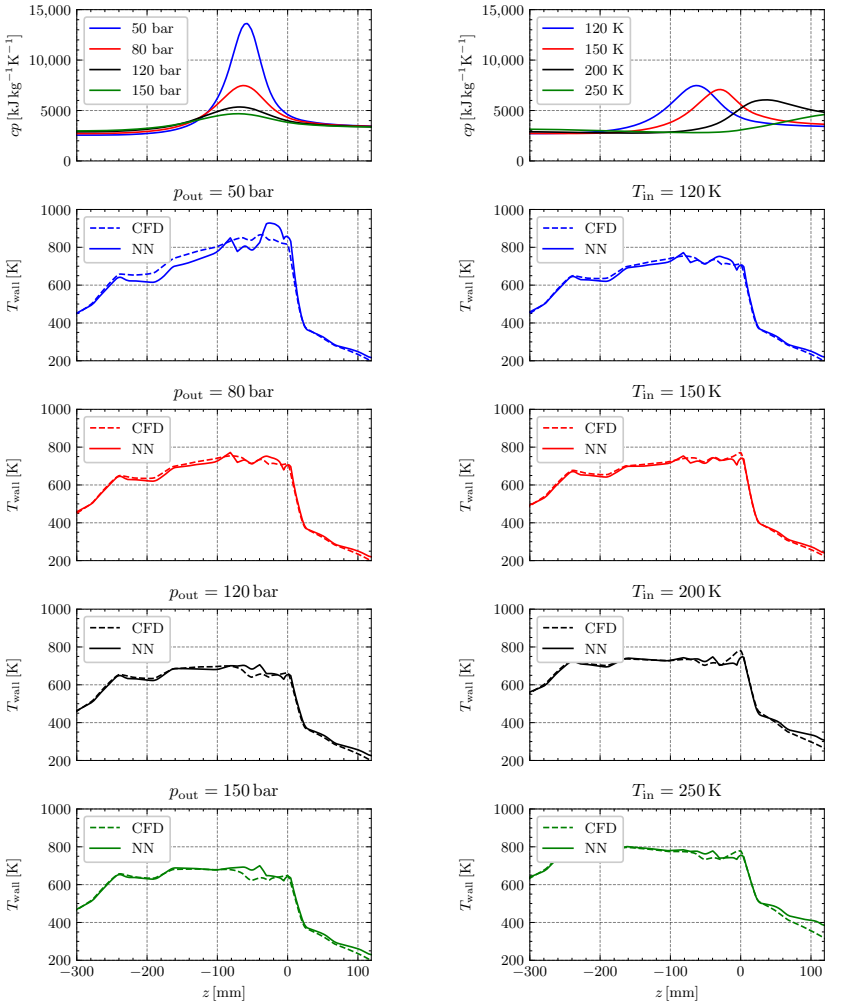

(**a**) (**b**)

Figure 9. Influence of temperature and pressure on the wall temperature prediction. (**a**) Outlet pressure variations for $T_{\mathrm{in}} = 120\,\mathrm{K}, \dot{m} = 2.6\,\mathrm{kg\,s^{-1}}, \dot{q}_{\mathrm{max}} = 51\,\mathrm{MW\,m^{-2}}$. (**b**) Inlet temperature variations for $p_{\mathrm{out}} = 80\,\mathrm{bar}, \dot{m} = 2.6\,\mathrm{kg\,s^{-1}}, \dot{q}_{\mathrm{max}} = 51\,\mathrm{MW\,m^{-2}}$.

4.3.4. Comparison to Original Surrogate Model

In Figure 10, the modified neural network, which considers curvature and fin thickness effects, and the original model without these inputs (NN-straight) are compared. The original network exhibits a significant error in the throat region, where it overestimates the wall temperature due to the missing curvature effect that increases heat transfer. In the cylindrical part, it underestimates the wall temperature, as it was not trained for the 2 mm fin thickness.

By considering curvature effects, the maximum error is reduced from 176 K to 40 K for the extended and modified model. This makes sense as the largest error occurs in the curved channel segments close to the nozzle throat and the extended model is trained for curvature. Additionally, the prediction for regions with a different fin thickness, such as the cylindrical part, also improves.

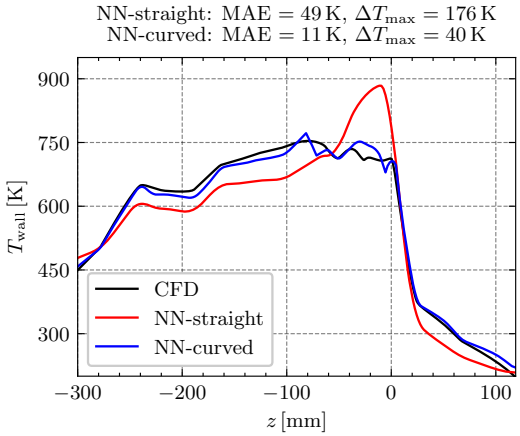

Figure 10. Comparison between the original model [2] and the extended model.

5. Discussion

Our extension of the surrogate model improves predictions for more realistic cooling channel flows, but remaining deviations are observed after strong changes in channel geometry and curvature, indicating the influence of inertia effects. These effects occur when the flow cannot fully develop due to geometry jumps, resulting in a different flow development for a locally identical cross-section. To accurately predict heat transfer, this behavior must be considered. In the following, we therefore propose a methodology to integrate the inertia effects directly into the neural network.

First, it is essential that all effects that play a role in the application also occur in the training data. Further CFD simulations with varying boundary conditions and geometry, e.g., a continuously changing curvature, are needed. Cooling channels with changing boundary conditions and geometry should be suitable to learn the local effects, e.g., of geometry changes. For an economic generation of these calculations, a parametric CAD approach followed by automatic meshing should be used.

Second, the neural network should be supplied with the geometry and thermodynamic states from data points upstream for each data point. With this additional information, the network is able to learn the effects of changes that occur upstream and influence the heat transfer. Two possibilities are immediately apparent. One approach is to stack the input vector from multiple sections through the channel.

A more sophisticated but definitely more elegant method is to use recurrent neural networks also known as RNNs [28]. RNNs are a generalization of feed-forward neural networks which contain memory and are best suited for sequential data, while RNNs perform the same function for every input vector the output of the current input also depends on past computations. Put differently, while making a decision, a RNN takes into consideration the current input and also what it has learned from the inputs it received previously.

Convolutional neural networks (CNNs) [29] are also successfully used for sequence prediction and would be another option. There are different types of RNNs and CNNs, which also depend on various hyperparameters. As a result, the design decisions also need to be analyzed or optimized, but with this approach it should definitely be possible to integrate information from the upstream area into the prediction. In our case, we could use such architectures to include inertia effects. Either way, it is impressive how far you can get with the very simple method presented in this paper.

6. Outlook

In addition to synthetic data from CFD, experimental data could be utilized. The HARCC data set [30] includes 6400 data points for methane and could be used for fine-tuning. Both data sets (synthetic and experimental) have individual advantages and disadvantages. Synthetic data always contains a systematic error based on the chosen CFD model. On the other hand, a large amount of data can be generated by simulation. Experimental data are subject to uncertainties of the measurements. The greatest disadvantage is the small number of experimental data points. For this reason, we will investigate whether training with synthetic data and fine-tuning with experimental data can combine both advantages. Furthermore, the influence of the data set size and data distribution on the performance of the surrogate models should be studied.

It could also be interesting to study the influence of impurities present in liquid methane on the cooling channel performance. Liquid methane mixtures contain small quantities of other elements (nitrogen, ethane, propane, carbon dioxide, and a small number of higher hydrocarbons) [31], which influence the thermodynamic properties of the mixture and might influence the heat transfer process close to the critical point. The influence of impurities could be included into the network architecture.

Author Contributions: Conceptualization, K.D. and G.W.-W.; Data curation, K.D.; Investigation, K.D.; Methodology, K.D. and G.W.-W.; Project administration, J.D.; Software, K.D.; Supervision, J.D.; Visualization, K.D.; Writing—original draft, K.D. and G.W.-W.; Writing—review and editing, K.D., E.K. and G.W.-W. All authors have read and agreed to the published version of the manuscript.

Funding: This research received no external funding.

Data Availability Statement: The data presented in this study are available on request from the corresponding author. The data are not publicly available due to confidentiality.

Acknowledgments: It is a pleasure to thank our former students Lukas Jakobs and Arnulf Rosner for their analysis of the data-based modeling approach.

Conflicts of Interest: The authors declare no conflict of interest.

Appendix A

Data for curved channel flows and flows with different fin thicknesses are generated using different channel geometries, as shown in Tables A1 and A2.

Table A1. Geometry of newly generated curved cooling channels.

A [mm^2]	AR [mm]	Fin [mm]	R [mm]	Hot-Gas Wall [mm]
1.5	1.5	1	±25	0.94
5	3.5	1	±30	1.00
2	1	1	±40	0.90
4	6	1	±50	1.00
3	2.5	1	±75	1.00
5	3.5	1	±100	1.00
7	8	1	±150	1.05
1.8	1.8	0.75	±30	0.90
4.3	9.7	1.5	±60	0.95

Table A2. Geometry of newly generated straight cooling channels.

A [mm^2]	AR [mm]	Fin [mm]	Hot-Gas Wall [mm]
2.2	1.5	0.75	0.85
3.5	4.4	1.5	1.05
6.7	6.1	2.0	0.97
8.2	8.5	2.5	1.10
9.4	1.2	3.5	0.92

Figure A1. LUMEN copper liner with milled cooling channels [8].

Table A3. Mean value and percentiles of the training data.

	T_b [K]	h_b [$\frac{kJ}{kg}$]	p_b [bar]	G [$\frac{kg}{s\,m^2}$]	$\dot{q}$ [$\frac{MW}{m^2}$]	r [µm]	A [mm^2]	AR [-]	d [mm]	T_w [K]
Mean	249	556	129	17,786	38	7.1	6.1	4.5	1.0	687
1%	123	56	48	3026	6	0.2	1	1.0	0.8	227
25%	181	271	92	11,600	13	1.2	5	1.7	1.0	453
50%	235	552	124	17,500	30	5.0	5	3.5	1.0	649
75%	303	791	162	22,500	50	13.8	10	9.8	1.05	877
99%	431	1170	221	45,000	82	20.0	10	9.8	1.2	1494

References

1. Nasuti, F.; Pizzarelli, M. Pseudo-Boiling and Heat Transfer Deterioration While Heating Supercritical Liquid Rocket Engine Propellants. *J. Supercrit. Fluids* **2021**, *168*, 105066. [CrossRef]
2. Waxenegger-Wilfing, G.; Dresia, K.; Deeken, J.C.; Oschwald, M. Heat Transfer Prediction for Methane in Regenerative Cooling Channels with Neural Networks. *J. Thermophys. Heat Transf.* **2020**, *34*, 347–357. [CrossRef]
3. Dresia, K. Prediction of Heat Transfer in Methane for Liquid Rocket Engines Using Artificial Neural Networks. Master's Thesis, RWTH Aachen, Aachen, Germany, 2018.
4. Dresia, K.; Waxenegger-Wilfing, G.; Riccius, J.; Deeken, J.; Oschwald, M. Numerically Efficient Fatigue Life Prediction of Rocket Combustion Chambers Using Artificial Neural Networks. In Proceedings of the 8th European Conference for Aeronautics and Space Sciences 2019 (EUCASS), Madrid, Spain, 1–4 July 2019. [CrossRef]
5. Jakobs, L. Validierung Eines Neuronalen Netzes {zur} Wärmeübergangsvorhersage in Kühlkanälen Anhand Realistischer Brennkammeranordnungen Unter Berücksichtigung von Krümmungseffekten Und Variablen Rippenstärken. Master's Thesis, RWTH Aachen University, Aachen, Germany, 2020.
6. Rosner, A. Vorhersage Des Wärmeübergangs in Raketenbrennkammern Mithilfe Neuronaler Netze Auf Basis Simulativer Und Experimenteller Daten. Bachelor's Thesis, RWTH Aachen University, Aachen, Germany, 2021.

7. Waxenegger-Wilfing, G.; Dresia, K.; Deeken, J.; Oschwald, M. Machine Learning Methods for the Design and Operation of Liquid Rocket Engines–Research Activities at the DLR Institute of Space Propulsion. In Proceedings of the Space Propulsion 2020+1 Conference, Virtual, 17–19 March 2021.
8. Haemisch, J.; Suslov, D.; Waxenegger-Wilfing, G.; Dresia, K.; Oschwald, M. LUMEN–Design of the Regenerative Cooling System for an Expander Bleed Cycle Engine Using Methane. In Proceedings of the Space Propulsion 2020+1 Conference, Virtual, 17–19 March 2021.
9. Deeken, J.; Waxenegger-Wilfing, G.; Oschwald, M.; Schlechtriem, S. LUMEN Demonstrator–Project Overview. In Proceedings of the Space Propulsion 2021 Conference, Virtual, 17–19 March 2021.
10. Pizzarelli, M.; Nasuti, F.; Onofri, M.; Roncioni, P.; Votta, R.; Battista, F. Heat Transfer Modeling for Supercritical Methane Flowing in Rocket Engine Cooling Channels. *Appl. Therm. Eng.* **2015**, *75*, 600–607. [CrossRef]
11. Pizzarelli, M.; Nasuti, F.; Onofri, M. Effect of Cooling Channel Aspect Ratio on Rocket Thermal Behavior. *J. Thermophys. Heat Transf.* **2014**, *28*, 410–416. [CrossRef]
12. DiValentin, J.; Naraghi, M. Effects Cooling Channel Curvature on Coolant Secondary Flow and Heat Transfer. In Proceedings of the 46th AIAA/ASME/SAE/ASEE Joint Propulsion Conference, Nashville, TN, USA, 25–28 July 2010; American Institute of Aeronautics and Astronautics: Nashville, TN, USA, 2010. [CrossRef]
13. Huzel, D.K.; Huang, D.H. *Modern Engineering for Design of Liquid-Propellant Rocket Engines*; AIAA: Reston, VA, USA, 1992.
14. Dittus, F.; Boelter, L. Heat Transfer in Automobile Radiators of the Tubular Type. *Int. Commun. Heat Mass Transf.* **1985**, *12*, 3–22. [CrossRef]
15. Shokri, M.; Ebrahimi, A. Improvement of Heat-Transfer Correlations for Supercritical Methane Coolant in Rectangular Channel. *Appl. Therm. Eng.* **2019**, *147*, 216–230. [CrossRef]
16. Zhang, M.; Sun, B. Improved Heat-Transfer Correlation for Transcritical Methane Based on a Velocity Profile Correction Term. *J. Therm. Sci. Eng. Appl.* **2022**, *14*, 041002. [CrossRef]
17. Latini, B.; Fiore, M.; Nasuti, F. Modeling Liquid Rocket Engine Coolant Flow and Heat Transfer in High Roughness Channels. *Aerosp. Sci. Technol.* **2022**, *126*, 107672. [CrossRef]
18. Sun, B.; Zhang, M.; Zhang, M.; Yuan, J. Coupled Numerical Analysis of Variable Cross-Section Cooling Channels in LOX/Methane Rocket Engines. *Heat Transf. Res.* **2020**, *51*, 1181–1196. [CrossRef]
19. Chen, Y.; Ma, Y.; Li, S.; He, D. Thermal Oscillation Behavior Profiling of Supercritical Methane in Cooling Rocket Engines. *Appl. Therm. Eng.* **2022**, *213*, 118779. [CrossRef]
20. Goodfellow, I.; Bengio, Y.; Courville, A. *Deep Learning*; The MIT Press: Cambridge, MA, USA, 2017.
21. Zapata Usandivaras, J.F.; Urbano, A.; Bauerheim, M.; Cuenot, B. Data Driven Models for the Design of Rocket Injector Elements. *Aerospace* **2022**, *9*, 594. [CrossRef]
22. Xu, S.; Wang, C.; Yang, C. Optimal Design of Regenerative Cooling Structure Based on Backpropagation Neural Network. *J. Thermophys. Heat Transf.* **2022**, *36*, 637–649. [CrossRef]
23. Brunton, S.L.; Noack, B.R.; Koumoutsakos, P. Machine Learning for Fluid Mechanics. *Annu. Rev. Fluid Mech.* **2020**, *52*, 477–508. [CrossRef]
24. Cai, S.; Mao, Z.; Wang, Z.; Yin, M.; Karniadakis, G.E. Physics-Informed Neural Networks (PINNs) for Fluid Mechanics: A Review. *Acta Mech. Sin.* **2021**, *37*, 1727–1738. [CrossRef]
25. Churchill, S. Friction Factor Equation Spans All Fluid-Flow Regimes. *Chem. Eng. J.* **1977**, *84*, 91–92.
26. Haemisch, J. *Heat Transfer Processes for Hydrogen and Methane in Cooling Channels of Regeneratively Cooled Thrust Chambers of Cryogenic Rocket Engines*; Technical Report; RWTH Aachen University: Aachen, Germany, 2020.
27. Linstrom, P. *NIST Chemistry WebBook: NIST Standard Reference Database, Database 69 (Online Database)*; National Institute of Standards and Technology: Gaithersburg, MD, USA, 1997. [CrossRef]
28. Sherstinsky, A. Fundamentals of Recurrent Neural Network (RNN) and Long Short-Term Memory (LSTM) Network. *Phys. D Nonlinear Phenom.* **2020**, *404*, 132306. [CrossRef]
29. O'Shea, K.; Nash, R. An Introduction to Convolutional Neural Networks. *arXiv* **2015**, arXiv:1511.08458v2.
30. Haemisch, J.; Suslov, D.; Oschwald, M. Experimental Study of Methane Heat Transfer Deterioration in a Subscale Combustion Chamber. *J. Propuls. Power* **2019**, *35*, 819–826. [CrossRef]
31. van Schyndel, J.; Goos, E.; Naumann, C.; Hardi, J.S.; Oschwald, M. Effects of Compounds in Liquefied Methane on Rocket Engine Operation. *Aerospace* **2022**, *9*, 698. [CrossRef]